

Effect of O-doping or N-vacancy on the structural, electronic and magnetic properties of MoSi_2N_4 monolayer

Yan-Tong Bian,¹ Guang-Hua Liu,^{a)} Sheng-Hui Qian, Xin-Xin Ding, Jia-Xi Gao, and Hao-Xuan Liu
School of Physical Science and Technology, Tiangong University, Tianjin 300387, China

(Dated: 2 December 2021)

In this letter, the effect of four types of defects (O_{Nout} , O_{Nin} , V_{Nout} and V_{Nin}) on the structural, electronic and magnetic properties of MoSi_2N_4 monolayer were investigated using first-principles calculations. The calculated results reveal that all the four types of defects lead to structural distortions around the O-dopant or N-vacancy, and thereby change the lattice parameter a' and monolayer height h . Specifically, O_{Nout} or O_{Nin} increases the lattice parameter, but V_{Nout} or V_{Nin} is on the contrary. O_{Nout} or V_{Nout} increases the monolayer height, whereas the height decreases for O_{Nin} or V_{Nin} . Each of the four types of defects has a fundamental effect on the electronic properties of MoSi_2N_4 monolayer, which can induce a transition from semiconductor to metal. O_{Nin} or V_{Nin} plays a vital role in the occurrence of a transition from non-magnetism to ferrimagnetism in MoSi_2N_4 monolayer. The effect of biaxial strain on the magnetic properties of the two systems with O_{Nin} and V_{Nin} was subsequently investigated. It is found that the total magnetic moments are less sensitive to biaxial strain whereas the local magnetic moments residing on the Mo atoms are increased for the two systems with O_{Nin} and V_{Nin} , as strain increases from -3% to 10% and from -9% to 10%, respectively. Furthermore, the magnetic phase transitions between ferrimagnetic and paramagnetic states were found to occur around -4% strain and within the range of -10% ~ -9% for the two systems with O_{Nin} and V_{Nin} , respectively. This study may provide a guidance for the application of MoSi_2N_4 monolayer in the spintronic and magnetic materials.

Two-dimensional (2D) materials, exhibiting physical and chemical properties that are richer than and completely different from the 3D bulk crystals due to the inherent quantum confinement effect along the direction of atomic-layered height, and thus have drawn considerable attentions from the scientific and industrial circles on a global scale in the past few years. The most typical and also earliest 2D material confirmed experimentally is graphene¹, which possesses unique electrical properties. Researchers subsequently got inspirations from it and developed a series of new 2D materials with excellent mechanical, thermodynamic, electrical, optical and magnetic properties, opening up another valuable path for the development and investigation of high-performance electronic devices, optoelectronic devices, spintronic devices, as well as energy conversion and storage fields²⁻⁵.

The MoSi_2N_4 compound, a novel synthetic 2D layered van der Waals (vdW) material without known 3D layered parents fabricated very recently by Hong *et al.*⁶ through chemical vapor deposition (CVD) technology, are attracting great interest in the optoelectronics, valleytronics, spintronics and so on. The synthesis of such material provides a huge opportunity for engineering materials with new attributes and functionality⁷. Hong *et al.* studied the MoSi_2N_4 monolayer film and reported that it is built up by septuple-atomic-layer of N-Si-N-Mo-N-Si-N, and exhibits non-magnetic semiconducting nature, high strength, as well as excellent ambient stability. They investigated its optical properties and evaluated the band gap via Tauc plot analysis further, and employed density functional theory (DFT)^{8,9} to explain observed phenomena. It is found that the MoSi_2N_4 monolayer possesses an indirect band gap of 1.94 eV and displays a high optical transmittance with an average of $97.5 \pm 0.2\%$ in the visible range, and the spin-orbit

coupling (SOC) existing in the valence band (VB) can be used to elucidate the two sub-peaks in the optical absorption spectrum. Wang *et al.*¹⁰ analyzed the crystal structure possessing septuple-atomic-layered characteristic for the MoSi_2N_4 monolayer and reported that it can be viewed as the insertion of the triple-atomic-layered $2H\text{-MoS}_2$ -type MoN_2 monolayer into the quadruple-atomic-layered $\alpha\text{-InSe}$ -type Si_2N_2 monolayer. The piezoelectric and electronic properties of MoSi_2N_4 monolayer under strain within the range from -4% to 4% were studied by Guo *et al.*¹¹ and found that the biaxial tensile strain can enhance the piezoelectric strain coefficient d_{11} and spin-orbit splitting at K point, whereas the band gap decreases with increasing strain. Guo *et al.*¹² investigated the effect of large biaxial strain ranging from -10% to 10% on the electronic structure, transport and piezoelectric coefficients of MoSi_2N_4 monolayer and reported that as strain increases from -10% to 10%, the band gap first increases and then decreases. Bafekry *et al.*¹³ explored the structural, mechanical, thermal, electronic, optical and photocatalytic properties of MoSi_2N_4 monolayer and found that it possesses a good thermoelectric performance, and its work function is very similar to that of phosphorene and MoS_2 monolayers. Kang *et al.*¹⁴ studied the second harmonic generation (SHG) effects of typical MoSi_2N_4 phases and reported that the two most typical phases may exhibit different SHG intensities due to the difference in P between the outer and inner layers of the sandwich structure. Li *et al.*¹⁵ and Yang *et al.*¹⁶ explored the valley-dependent properties of MoSi_2N_4 monolayer and found that it is a semiconductor with a pair of Dirac-type valleys located at the corners of the hexagonal Brillouin zone and can realize the valley-contrast properties, suggesting that its potential applications in valleytronic and spintronic devices. Moreover, Cao *et al.*¹⁷ investigated the vdW heterostructures composed of MoSi_2N_4 vertically contacted by graphene and NbS_2 monolayers and showed that $\text{MoSi}_2\text{N}_4/\text{NbS}_2$ contact exhibits an ultralow Schottky barrier height (SBH), and the SBH can

^{a)}Electronic mail: liuguanghua@tiangong.edu.cn

be modulated via interlayer distance or external electric fields for MoSi₂N₄/graphene contact, opening up an opportunity for reconfigurable and tunable nanoelectronic devices.

As is well known, the physical and chemical properties of 2D materials under diverse conditions and requirements can commonly be effectively modulated by using of defect, strain, external electric field^{18–27} and so on, which provides convenience for investigating the optical, electrical, magnetic and topological properties etcetera closely related to the electronic structure. Despite an increasing theoretical exploration toward MoSi₂N₄ monolayer recently, to date the effect of defect on its physical properties has not yet been investigated. Besides, such work is significant to understand the natures of MoSi₂N₄ compound and develop its practical applications further.

In view of the facts, herein we targeted to view the structural, electronic and magnetic properties of MoSi₂N₄ monolayer induced by the defects with O-doping and N-vacancy using first-principles approach based on DFT. The electronic and magnetic properties were studied through GGA + SOC and GGA + Spin Polarization calculations, respectively. The calculated results of intrinsic MoSi₂N₄ monolayer were also given in this letter for comparison.

Considering that there are two types of N atomic layers according to the symmetry of septuple-atomic-layered MoSi₂N₄ monolayer, namely the outer and inner layers, which were respectively marked with N_{out} and N_{in} in Fig. 1(a) for the convenience of description. For the substitutional doping type of defects, the O atom is treated as dopant to substitute for one N atom in the N_{out} and N_{in} respectively, which were respectively denoted as O_{Nout} and O_{Nin}. The vacancy type of defects come from the removal of one N atom in the N_{out} and N_{in} respectively, which were respectively labeled as V_{Nout} and V_{Nin}. Therefore there are four types of defects. The concentrations of these defects were all set to 6.25%, corresponding to the 2 × 2 × 1 super-cell. Throughout our calculations, the plane-wave pseudopotential method²⁸ within the framework of DFT implemented in the CASTEP code²⁹ was adopted. Norm-conserving pseudopotentials were applied to describe the interactions between ion-cores and valence electrons, and the generalized gradient approximation (GGA) functional following the Perdew-Burke-Ernzerhof (PBE)³⁰ scheme was employed to paint the electronic exchange-correlation potential. In order to minimize the interaction between the periodic layers along the c-axis direction, the vacuum slab of more than 24 Å between layers was adopted. All geometric structures were fully relaxed until the maximum force on each atom is less than 0.01 eV/Å. The cut-off energy for plan-wave expansion was set to 1100 eV and the Monkhorst-Pack³¹ **k**-point grid of 11 × 11 × 1 in the Brillouin zone was applied to both the structural relaxation and self-consistent field (SCF) process with a convergence threshold of 1.0 × 10^{−7} eV/atom.

Figs. 1(a) and 1(b) present the side and top views of intrinsic MoSi₂N₄ monolayer respectively, which belongs to the hexagonal lattice with the P-6M2 space group (No. 187). The lattice parameter a ($a = b$) of the unit cell, monolayer height h and cohesive energy E_{coh} for intrinsic MoSi₂N₄ monolayer were calculated first to examine the validity of the DFT-PBE

method employed in this letter. The calculated a , h and E_{coh} are respectively 2.932 Å, 7.075 Å and -8.573 eV/atom, which agree well with previous values^{6,11,13,15,17,32}, indicating the accuracy of this method. Tab. I summarizes the Si-Si distances (labeled as d_{Si} in Fig. 1(b)) nearest to the O-dopant or N-vacancy in the N_{out}, Mo-Mo distances (labeled as d_{Mo} in Fig. 1(b)) nearest to the O-dopant or N-vacancy in the N_{in}, lattice parameter a' ($a' = b'$) of the 2 × 2 × 1 super-cell and monolayer height h for intrinsic and four defective systems. It is clear from this table that the d_{Si} in the system with O_{Nout} and d_{Mo} in the system with O_{Nin} increase, whereas the d_{Si} in the system with V_{Nout} and d_{Mo} in the system with V_{Nin} decrease, compared with those of intrinsic system. Moreover, a little bigger for the system with O_{Nout} or O_{Nin} toward the lattice parameter a' than intrinsic system, yet the reduction of a' was found in the system with V_{Nout} or V_{Nin}. In addition, all the four types of defects can also have an effect on the height h of MoSi₂N₄ monolayer. From Tab. I, the height h of the system with O_{Nout} or V_{Nout} is greater than that of intrinsic system. Nevertheless, the h becomes smaller for the system with O_{Nin} or V_{Nin}. It is shown that the increase or decrease of h may be independent of the implementation of O-doping or N-vacancy, which is only related to which N atomic layer the O-doping or N-vacancy actualized in. Furthermore, the monolayer height will increase for O-doping or N-vacancy actualized in the N_{out}; on the contrary, it will decrease for that implemented in the N_{in}.

The calculated electronic band structures along the high symmetric paths in the 1st Brillouin zone (Fig. 1(c)) and corresponding total density of states (TDOS) incorporating SOC of intrinsic and four defective systems are displayed in Figs. 2(a) ~ 2(e), respectively. For the intrinsic system, the valence band maximum (VBM) is located at the Γ point whereas the conduction band minimum (CBM) is located at the K point, indicating an indirect band gap semiconductor characteristic (see Fig. 2(a)). The calculated band gap value is 1.953 eV, which is in good accordance with previous result (1.940 eV) evaluated by Hong *et al.*⁶ through Tauc plot analysis. Furthermore, the calculated spin-orbit splitting in the VB at K point is 126 meV, which is highly consistent with previous data available^{6,11,12,15}. Interestingly enough, a transition from semiconductor to metal induced by each of the four types of defects was observed in MoSi₂N₄ monolayer. In other words, for the system with O_{Nout}, O_{Nin}, V_{Nout} or V_{Nin}, it is quite evident that each of them exhibits metallic characteristic with two dispersive energy band passing over the Fermi level (see Figs. 2(b) ~ 2(e)). Moreover, the spin-orbit splitting values are respectively 130, 120, 126 and 100 meV for the four systems with O_{Nout}, O_{Nin}, V_{Nout} and V_{Nin}. Compared with the splitting value of intrinsic system, there is a tiny increasement for that of the system with O_{Nout}. But for the system with O_{Nin} or V_{Nin}, the splitting value decreases. It is suggested that all the O_{Nout}, O_{Nin} and V_{Nin} have a marginal effect on the spin-orbit coupling in MoSi₂N₄ monolayer.

We detected the Mulliken overlap populations³³ between the center N atom in the N_{out} and its three Si ligands, the center N atom in the N_{in} and its three Mo ligands for the intrinsic system further. It is found that the average overlap popula-

tions of the three N-Si and three N-Mo bonds are 1.45 and 0.94, respectively. The absolute values of the overlap populations reflect the level of covalent properties for the N-Si and N-Mo bonds, and also mean the extent of the electron sharing between them. However, the average overlap populations of the three O-Si bonds in the system with O_{Nout} and three O-Mo bonds in the system with O_{Nin} are -0.25 and -0.02, respectively. It is shown that both the O-Si and O-Mo bonds exhibit antibonding states, implying there exist repulsive interactions, which may be the causes for the larger d_{Si} in the system with O_{Nout} , d_{Mo} in the system with O_{Nin} and a' in the two systems with O_{Nout} and O_{Nin} . Conversely, the removal of one N atom in the N_{out} or N_{in} from the intrinsic $MoSi_2N_4$ monolayer causes structural constrictions of the three Si atoms or three Mo atoms surrounding the N-vacancy. Three bonding electrons in the system with V_{Nout} or four bonding electrons in the system with V_{Nin} are removed while the formation of N-vacancy. Such a close neighbor of the vacancy of the Si atoms or Mo atoms will appear three effective charges of dangling bonds. For the intrinsic system, the average charges of the three Si atoms directly bonding with the center N atom in the N_{out} and three Mo atoms directly bonding with that in the N_{in} are respectively 1.03e and 0.06e, according to the calculated Mulliken atomic populations. Nonetheless, the average charge of 0.64e was observed on the three Si atoms nearest to the N-vacancy in the system with V_{Nout} , and the average charge of the three Mo atoms nearest to the N-vacancy in the system with V_{Nin} is -0.06e. It is shown that the electron density residing on the three Si atoms or three Mo atoms is increased. Such charge redistribution can be seen as the micro-explanation for the reductions of d_{Si} in the system with V_{Nout} , d_{Mo} in the system with V_{Nin} and a' in the two systems with V_{Nout} and V_{Nin} .

The spin polarized calculations without SOC and given initial magnetic configuration were performed to analyze the magnetic behavior. According to the calculated Mulliken atomic populations, the total magnetic moments m_{tot} of intrinsic and four defective systems are also tabulated in Tab. I. From this table, the intrinsic $MoSi_2N_4$ monolayer possesses no magnetic moment, which is consistent with previous result calculated by Hong *et al.*⁶, showing that this calculation method is reliable. For the four defective systems, the total magnetic moment of the system with O_{Nout} or V_{Nout} is also zero. Nevertheless, a m_{tot} of $1.000\mu_B$ was observed in the system with O_{Nin} or V_{Nin} . As displayed in Fig. 3(a), the partial density of states (PDOS) of Mo and O atoms implies that the total magnetic moment mainly originates from the strong coupling between the 4d states of Mo and 2p state of O for the system with O_{Nin} . For the system with V_{Nin} , the PDOS of Mo and N atoms suggests that the total magnetic moment primarily comes from the strong coupling between the 4d states of Mo and 2p state of N, as shown in Fig. 3(b).

We inspected the local magnetic moments of the two systems with O_{Nin} and V_{Nin} further. Figs. 4(a) and 4(b) show the side views of net spin density for the two systems with O_{Nin} and V_{Nin} , respectively. As shown in these figures, the total magnetic moment is notably contributed from the local magnetic moments residing on the Mo atoms. Accord-

ing to these local magnetic moments, the magnetic structures for both of these systems can be demonstrated. Figs. 5(a) and 5(b) present the detailed magnetic moment arrangements within a super-cell in the two systems with O_{Nin} and V_{Nin} , respectively. From these figures, the local magnetic moments of Mo(1), Mo(2) and Mo(3) atoms around the O-dopant or N-vacancy are equivalent to each other, exhibiting up-spin states, and the magnitudes are $0.520\mu_B$ and $0.580\mu_B$ per Mo atom for the two systems with O_{Nin} and V_{Nin} , respectively. However, the remaining one Mo(4) atom possesses a local magnetic moment with down-spin state, and the magnitudes are $-0.470\mu_B$ and $-0.410\mu_B$ per Mo atom for the two systems with O_{Nin} and V_{Nin} , respectively. It can be concluded that such magnetic moment arrangement displays a magnetic structure with ferrimagnetic (FRM) ordering for the system with O_{Nin} or V_{Nin} .

In order to verify the magnetic structure further, two different initial magnetic configurations within the $2 \times 2 \times 1$ super-cells of the system with O_{Nin} or V_{Nin} were given, namely, one ferromagnetic (FM) and one antiferromagnetic (AFM) initial states (see Figs. 6(a) ~ 6(d)). We found that whatever the initial magnetic configuration is, the system with O_{Nin} or V_{Nin} becomes a ferrimagnetic state finally which is the same as that (see Figs. 5(a) and 5(b)) obtained using spin polarized calculations without given initial magnetic configuration. It is indicated that the system with O_{Nin} or V_{Nin} should possess a ferrimagnetic ground state.

Next, the effect of biaxial strain on the magnetic properties of the two systems with O_{Nin} and V_{Nin} was discussed. Here, the biaxial strain ε is defined as

$$\varepsilon = \frac{a' - a'_0}{a'_0} \times 100\%, \quad (1)$$

where a' and a'_0 are the strained and unstrained lattice parameters, respectively. The positive (negative) ε represents the tensile (compressive) strain, and a strain range from -10% to 10% was applied to both of these systems. Tab. II and Tab. III list the calculated total magnetic moment m_{tot} , local magnetic moments residing on the Mo atoms $m_{Mo(1)}$, $m_{Mo(2)}$, $m_{Mo(3)}$ and $m_{Mo(4)}$ of the two systems with O_{Nin} and V_{Nin} under different strains, respectively. From Tab. II, it is obvious that the system with O_{Nin} exhibits a ferrimagnetic state within the range of -3% ~ 10%. The variation of m_{tot} is negligible as strain increases from -3% to 10%, indicating that the m_{tot} is less sensitive to biaxial strain. Nevertheless, the $m_{Mo(1)}$, $m_{Mo(2)}$, $m_{Mo(3)}$ and $m_{Mo(4)}$ are all increased. It is worth noting that the local magnetic moments residing on the Mo(1), Mo(2) and Mo(3) atoms are still equivalent to each other, which may be associated with the unbroken lattice symmetry under biaxial strain. Moreover, the m_{tot} , $m_{Mo(1)}$, $m_{Mo(2)}$, $m_{Mo(3)}$ and $m_{Mo(4)}$ are all zero within the range of -10% ~ -5%, indicating this system shows a paramagnetic state. We found that the m_{tot} , $m_{Mo(1)}$, $m_{Mo(2)}$, $m_{Mo(3)}$ and $m_{Mo(4)}$ at -4% strain are all difficult to calculate, cannot be obtained, and thus the data at such strain are not given in Tab. II. Therefore we suggest that there exists a magnetic phase transition between ferrimagnetic and paramagnetic states around -4% strain. For the system with V_{Nin} , it is clear from Tab. III that it presents a ferrimagnetic state within the range of -9% ~ 10%. Analogously, the

m_{tot} is also less sensitive to biaxial strain, the $m_{Mo(1)}$, $m_{Mo(2)}$, $m_{Mo(3)}$ and $m_{Mo(4)}$ are all increased, the local magnetic moments of Mo(1), Mo(2) and Mo(3) atoms are still equivalent to each other, as strain increases from -9% to 10%. However, the m_{tot} , $m_{Mo(1)}$, $m_{Mo(2)}$, $m_{Mo(3)}$ and $m_{Mo(4)}$ are all zero at -10% strain, suggesting this system displays a paramagnetic state. We calculated these magnetic moments at -11% strain further and found that all of them are also zero. It is shown that there also exists a magnetic phase transition between ferrimagnetic and paramagnetic states within the range of -10% ~ -9%.

In conclusion, we systematically investigated the structural, electronic and magnetic properties of $MoSi_2N_4$ monolayer induced by the four types of defect (O_{Nout} , O_{Nin} , V_{Nout} and V_{Nin}), using first-principles density functional theory calculations. Our results reveal that all the four types of defects lead to structural distortions around the O-dopant or N-vacancy, and thereby change the lattice parameter a' and monolayer height h . Specifically, O_{Nout} or O_{Nin} increases the lattice parameter, but V_{Nout} or V_{Nin} is on the contrary. O_{Nout} or V_{Nout} increases the monolayer height, whereas the height decreases for O_{Nin} or V_{Nin} . Each of the four types of defects has a fundamental effect on the electronic properties of $MoSi_2N_4$ monolayer, which can induce a transition from semiconductor to metal. O_{Nin} or V_{Nin} plays a vital role in the occurrence of a transition from non-magnetism to ferrimagnetism in $MoSi_2N_4$ monolayer. Subsequently, the effect of biaxial strain on the magnetic properties of the two systems with O_{Nin} and V_{Nin} was investigated. It is found that the total magnetic moments are less sensitive to biaxial strain, the local magnetic moments residing on the Mo atoms are increased for the two systems with O_{Nin} and V_{Nin} , as strain increases from -3% to 10% and from -9% to 10%, respectively. Furthermore, the magnetic phase transitions between ferrimagnetic and paramagnetic states were found to occur around -4% strain and within the range of -10% ~ -9% for the two systems with O_{Nin} and V_{Nin} , respectively. This study may provide a guidance for the application of $MoSi_2N_4$ monolayer in the spintronic and magnetic materials.

- ¹K. S. Novoselov, A. K. Geim, S. V. Morozov, D. Jiang, Y. Zhang, S. V. Dubonos, I. V. Grigorieva, and A. A. Firsov. Electric field effect in atomically thin carbon films. *Science*, 306(5696):666–669, 2004.
- ²Chanyoung Yim, Kangho Lee, Niall McEvoy, Maria O'Brien, Sarah Riazimehr, Nina C. Berner, Conor P. Cullen, Jani Kotakoski, Jannik C. Meyer, Max C. Lemme, and Georg S. Duesberg. High-performance hybrid electronic devices from layered ptse2 films grown at low temperature. *ACS Nano*, 10(10):9550–9558, 2016. PMID: 27661979.
- ³Britton W. H. Baugher, Hugh O. H. Churchill, Yafang Yang, and Pablo Jarillo-Herrero. Optoelectronic devices based on electrically tunable p-n diodes in a monolayer dichalcogenide. *Nature Nanotechnology*, 9(4):262–267, Apr 2014.
- ⁴Kin Fai Mak, Keliang He, Jie Shan, and Tony F. Heinz. Control of valley polarization in monolayer mos2 by optical helicity. *Nature Nanotechnology*, 7(8):494–498, Aug 2012.
- ⁵Marco Bernardi, Maurizia Palummo, and Jeffrey C. Grossman. Extraordinary sunlight absorption and one nanometer thick photovoltaics using two-dimensional monolayer materials. *Nano Letters*, 13(8):3664–3670, 2013. PMID: 23750910.
- ⁶Yi-Lun Hong, Zhibo Liu, Lei Wang, Tianya Zhou, Wei Ma, Chuan Xu, Shun Feng, Long Chen, Mao-Lin Chen, Dong-Ming Sun, Xing-Qiu Chen, Hui-Ming Cheng, and Wencai Ren. Chemical vapor deposition of layered two-dimensional mosi2n4 materials. *Science*, 369(6504):670–674, 2020.

- ⁷Kostya S Novoselov. Discovery of 2D van der Waals layered $MoSi_2N_4$ family. *National Science Review*, 08 2020. nwaal190.
- ⁸P. Hohenberg and W. Kohn. Inhomogeneous electron gas. *Phys. Rev.*, 136:B864–B871, Nov 1964.
- ⁹W. Kohn and L. J. Sham. Self-consistent equations including exchange and correlation effects. *Phys. Rev.*, 140:A1133–A1138, Nov 1965.
- ¹⁰Lei Wang, Yongpeng Shi, Mingfeng Liu, Yi-Lun Hong, Ming-Xing Chen, Ronghan Li, Qiang Gao, Wencai Ren, Hui-Ming Cheng, Yiyi Li, and Xing-Qiu Chen. Structure-driven intercalated architecture of septuple-atomic-layer ma_{2-24} family with diverse properties from semiconductor to topological insulator to ising superconductor, 2020.
- ¹¹San-Dong Guo, Yu-Tong Zhu, and Wen-Qi Mu. Intrinsic piezoelectricity in monolayer $XS_i_2N_4$ (x=ti, zr, hf, cr, mo and w), 2020.
- ¹²Xiao-Shu Guo and San-Dong Guo. Tuning electronic structures, transport and piezoelectric coefficients of monolayer $MoSi_2N_4$ with biaxial strain, 2020.
- ¹³A. Bafekry, M. Faraji, Do M. Hoat, M. M. Fadlallah, M. Shahrokhi, F. Shojaei, D. Gogova, and M. Ghergherehchi. Mosi2n4 single-layer: a novel two-dimensional material with outstanding mechanical, thermal, electronic, optical, and photocatalytic properties, 2020.
- ¹⁴Lei Kang and Zhesuai Lin. Second harmonic generation of mosi2n4 layer, 2020.
- ¹⁵Si Li, Weikang Wu, Xiaolong Feng, Shan Guan, Wanxiang Feng, Yugui Yao, and Shengyuan A. Yang. Valley-dependent properties of monolayer $mosi_2n_4$, ws_2n_4 and $mosi_2as_4$, 2020.
- ¹⁶Chen Yang, Zhigang Song, Xiaotian Sun, and Jing Lu. Valley pseudospin in monolayer $mosi_2n_4$ and $mosi_2as_4$, 2020.
- ¹⁷Liemao Cao, Guanghui Zhou, L. K. Ang, and Yee Sin Ang. Two-dimensional van der waals electrical contact to monolayer $mosi_2n_4$, 2020.
- ¹⁸Hongliang Shi, Hui Pan, Yong-Wei Zhang, and Boris I. Yakobson. Quasiparticle band structures and optical properties of strained monolayer mos_2 and ws_2 . *Phys. Rev. B*, 87:155304, Apr 2013.
- ¹⁹Anne Marie Z. Tan, Christoph Freysoldt, and Richard G. Hennig. First-principles investigation of charged dopants and dopant-vacancy defect complexes in monolayer Mos_2 . *Phys. Rev. Materials*, 4:114002, Nov 2020.
- ²⁰Asadollah Bafekry, Chuong Van Nguyen, Catherine Stampfl, Berna Ak-genc, and Mitra Ghergherehchi. Oxygen vacancies in the single layer of ti_2co_2 mxene: Effects of gating voltage, mechanical strain, and atomic impurities. *physica status solidi (b)*, n/a(n/a):2000343, 2020.
- ²¹Aarti Shukla and N.K. Gaur. A dft study of defects in sno monolayer and their interaction with o2 molecule. *Chemical Physics Letters*, 754:137717, 2020.
- ²²Zhen Lin, Bin Fu, and Yukai An. Effects of defects and anions on the geometry, electronic structures and exchange interaction of fe-doped 2h-mose2 monolayer. *Applied Surface Science*, 528:146960, 2020.
- ²³Chen Wang and Yukai An. Effects of strain and stacking patterns on the electronic structure, valley polarization and magnetocrystalline anisotropy of layered vt_2e . *Applied Surface Science*, 538:148098, 2021.
- ²⁴Liangzhi Kou, Chun Tang, Yi Zhang, Thomas Heine, Changfeng Chen, and Thomas Frauenheim. Tuning magnetism and electronic phase transitions by strain and electric field in zigzag mos_2 nanoribbons. *The Journal of Physical Chemistry Letters*, 3(20):2934–2941, 2012. PMID: 26292229.
- ²⁵Ai-Ming Hu, Ling ling Wang, Wen-Zhi Xiao, and Bo Meng. Electronic structures and magnetic properties in cu-doped two-dimensional dichalcogenides. *Physica E: Low-dimensional Systems and Nanostructures*, 73:69–75, 2015.
- ²⁶Asadollah Bafekry, Saber Farjami Shayesteh, Mitra Ghergherehchi, and Francois M. Peeters. Tuning the bandgap and introducing magnetism into monolayer bc_3 by strain/defect engineering and adatom/molecule adsorption. *Journal of Applied Physics*, 126(14):144304, 2019.
- ²⁷Asadollah Bafekry, Catherine Stampfl, Mitra Ghergherehchi, and Saber Farjami Shayesteh. A first-principles study of the effects of atom impurities, defects, strain, electric field and layer thickness on the electronic and magnetic properties of the c_{2n} nanosheet. *Carbon*, 157:371–384, 2020.
- ²⁸M. C. Payne, M. P. Teter, D. C. Allan, T. A. Arias, and J. D. Joannopoulos. Iterative minimization techniques for ab initio total-energy calculations: molecular dynamics and conjugate gradients. *Rev. Mod. Phys.*, 64:1045–1097, Oct 1992.
- ²⁹S. J. Clark, M. D. Segall, C. J. Pickard, P. J. Hasnip, M. J. Probert, K. Refson, and M.C. Payne. First principles methods using CASTEP. *Z. Kristall.*,

220:567–570, 2005.

- ³⁰John P. Perdew, Kieron Burke, and Matthias Ernzerhof. Generalized gradient approximation made simple. *Phys. Rev. Lett.*, 77:3865–3868, Oct 1996.
- ³¹Hendrik J. Monkhorst and James D. Pack. Special points for brillouin-zone integrations. *Phys. Rev. B*, 13:5188–5192, Jun 1976.
- ³²Hongxia Zhong, Wenqi Xiong, Pengfei Lv, Jin Yu, and Shengjun Yuan. Strain-induced semiconductor to metal transition in ma2z4 bilayers, 2020.
- ³³M. D. Segall, R. Shah, C. J. Pickard, and M. C. Payne. Population analysis of plane-wave electronic structure calculations of bulk materials. *Phys. Rev. B*, 54:16317–16320, Dec 1996.

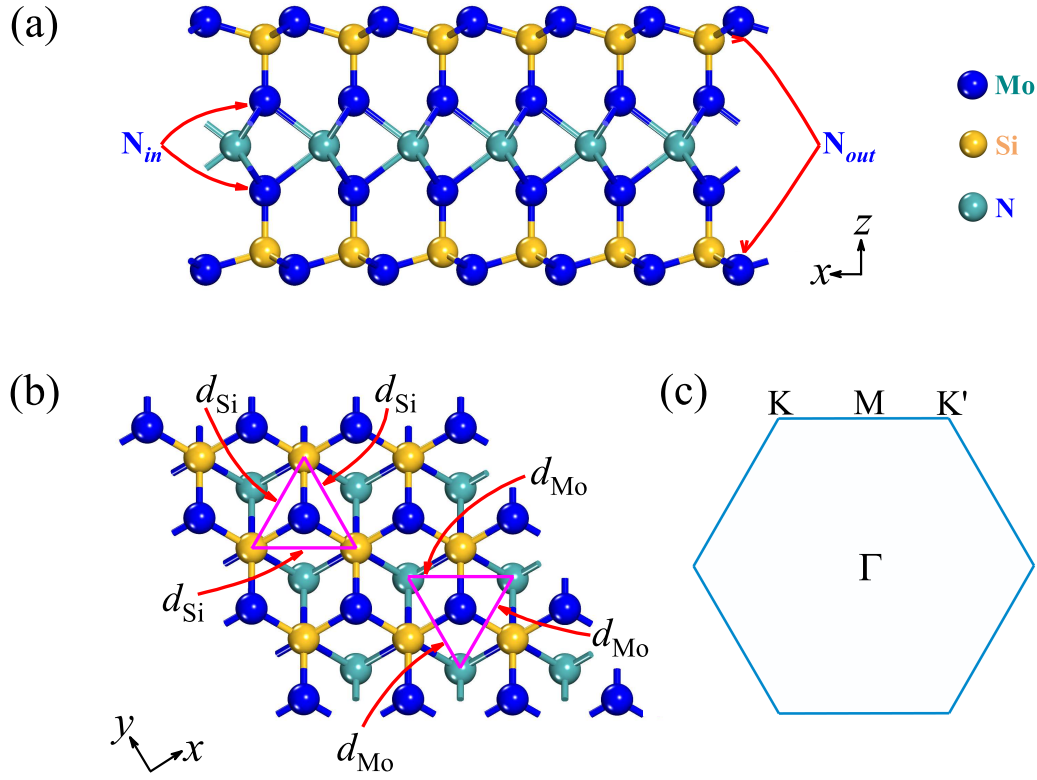


FIG. 1. (Color online) Views of intrinsic MoSi₂N₄ monolayer as seen from (a) side and (b) top; (c) 2D 1st Brillouin zone. (N_{out} and N_{in} represent the outer and inner N atomic layers, respectively; d_{Si} denotes the Si-Si distances nearest to the O-dopant or N-vacancy in the N_{out}; d_{Mo} marks the Mo-Mo distances nearest to the O-dopant or N-vacancy in the N_{in}.)

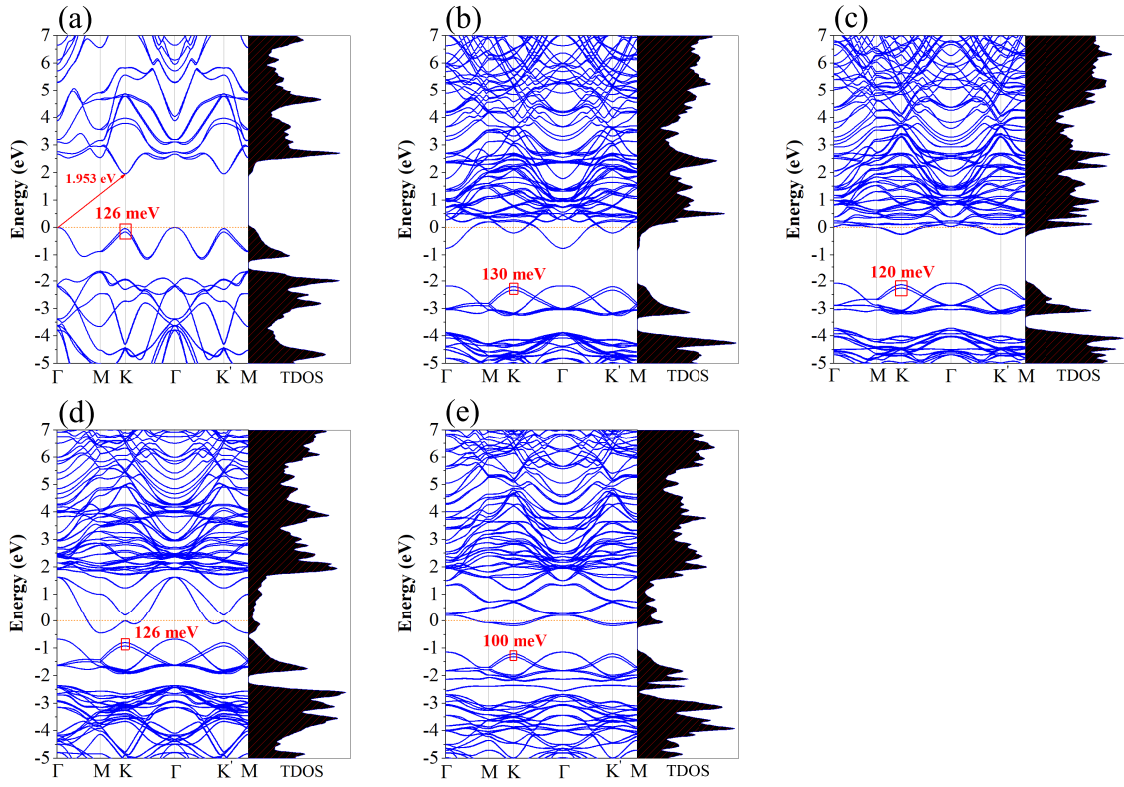


FIG. 2. (Color online) Electronic band structures and corresponding TDOS incorporating SOC in a representative window around the Fermi level (is set to 0 eV) of (a) intrinsic and four systems with (b) O_{Nout} , (c) O_{Nin} , (d) V_{Nout} and (e) V_{Nin} . (Red arrow and frames highlight the indirect band gap and spin-orbit splittings in the VB at K point, respectively.)

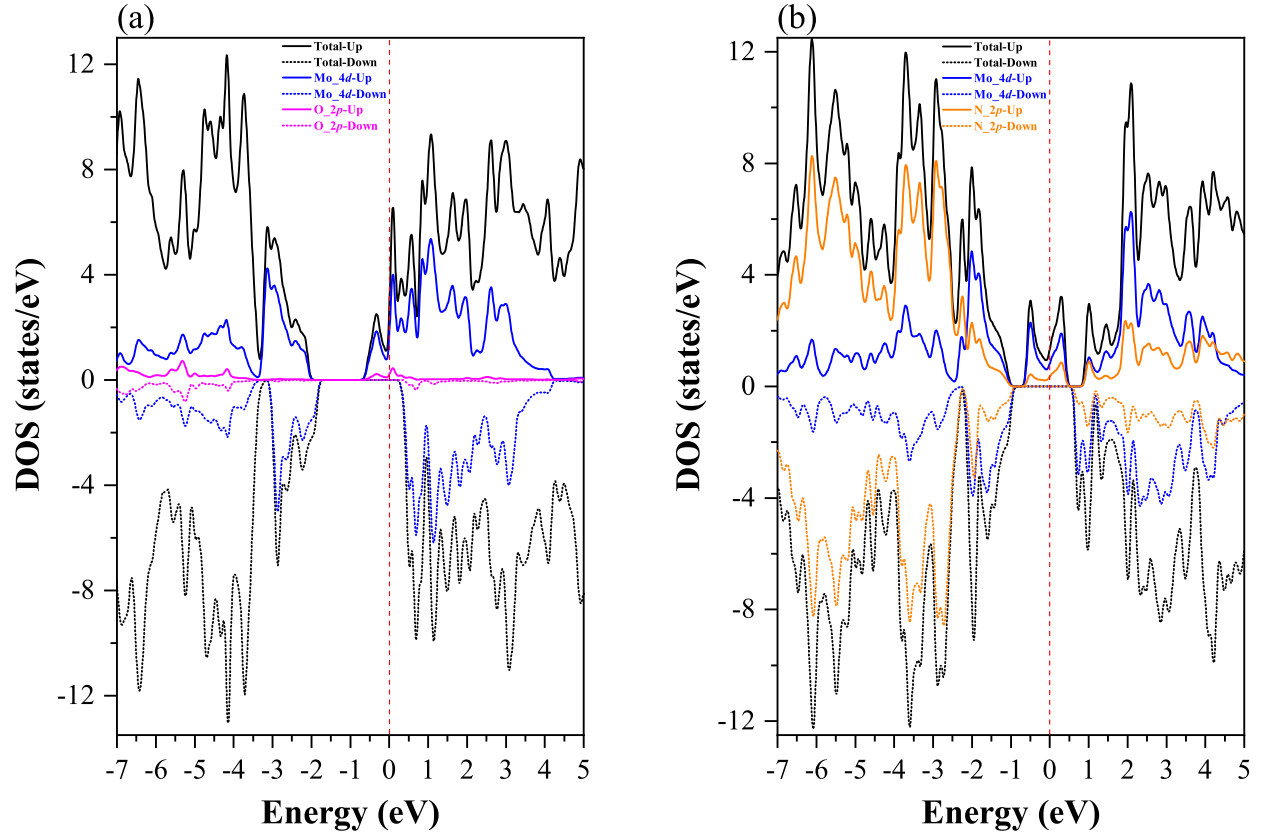


FIG. 3. (Color online) DOS projected on (a) Mo and O atoms in the system with O_{Nin} and (b) Mo and N atoms in the system with V_{Nin} .

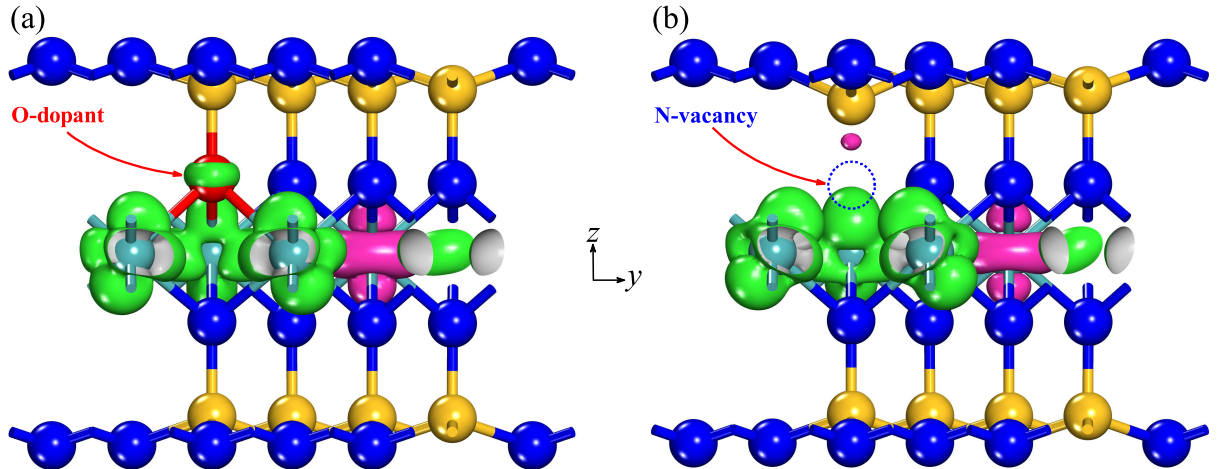


FIG. 4. (Color online) Side views of net spin density at an isovalue of $5 \times 10^{-2} e/\text{\AA}^3$ for the two systems with (a) O_{Nin} and (b) V_{Nin} . (The up-spin and down-spin states are denoted as green and magenta, respectively.)

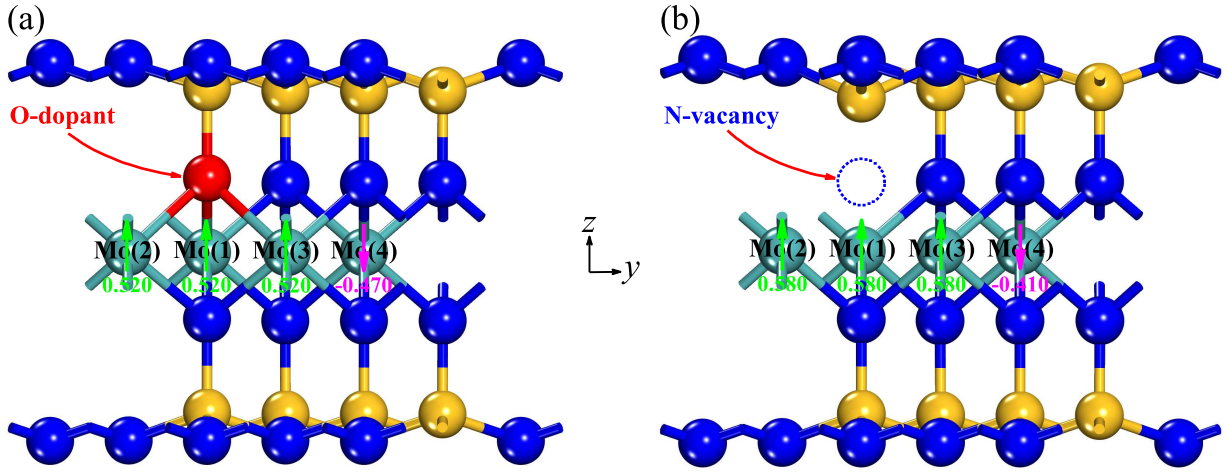


FIG. 5. (Color online) The detailed magnetic moment arrangements within a super-cell in the two systems with (a) O_{Nin} and (b) V_{Nin} .

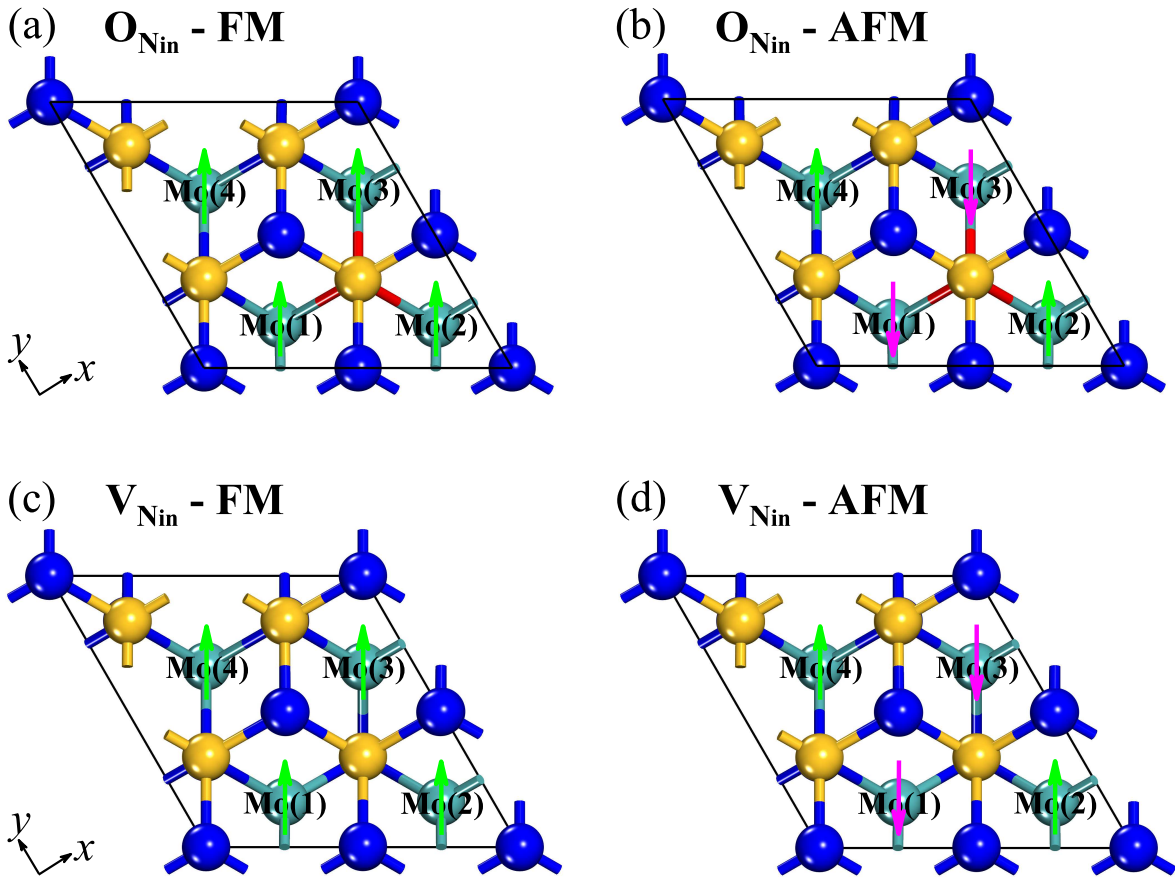


FIG. 6. (Color online) The given initial magnetic configurations of the two systems with O_{Nin} and V_{Nin} : two ferromagnetic states (a, c) and two antiferromagnetic states (b, d).

TABLE I. The Si-Si distances (d_{Si}) nearest to the O-dopant or N-vacancy in the N_{out} , Mo-Mo distances (d_{Mo}) nearest to the O-dopant or N-vacancy in the N_{in} , lattice parameters a' ($a' = b'$) of the $2 \times 2 \times 1$ super-cell, monolayer height h and total magnetic moment m_{tot} for intrinsic and four defective systems.

Systems	d_{Si} (Å)	d_{Mo} (Å)	a' (Å)	h (Å)	m_{tot} (μ_B /super-cell)
Intrinsic	2.932	2.932	5.864	7.075	0.000
O_{Nout}	3.060	—	5.887	7.092	0.000
O_{Nin}	—	2.989	5.884	7.067	1.000
V_{Nout}	2.856	—	5.856	7.103	0.000
V_{Nin}	—	2.917	5.850	7.065	1.000

TABLE II. The calculated total magnetic moment m_{tot} , local magnetic moments residing on the Mo atoms $m_{Mo(1)}$, $m_{Mo(2)}$, $m_{Mo(3)}$ and $m_{Mo(4)}$ of the system with O_{Nin} under different strains.

Strain	m_{tot} (μ_B /super-cell)	$m_{Mo(1)}$ (μ_B /atom)	$m_{Mo(2)}$ (μ_B /atom)	$m_{Mo(3)}$ (μ_B /atom)	$m_{Mo(4)}$ (μ_B /atom)
-10%	0.000	0.000	0.000	0.000	0.000
-8%	0.000	0.000	0.000	0.000	0.000
-6%	0.000	0.000	0.000	0.000	0.000
-5%	0.000	0.000	0.000	0.000	0.000
-4%	—	—	—	—	—
-3%	0.997	0.330	0.330	0.330	-0.120
-2%	1.000	0.340	0.340	0.340	-0.140
0	1.000	0.520	0.520	0.520	-0.470
2%	0.999	0.560	0.560	0.560	-0.510
4%	0.969	0.590	0.590	0.590	-0.590
6%	0.975	0.680	0.680	0.680	-0.820
8%	1.000	0.880	0.880	0.880	-1.340
10%	1.000	1.100	1.100	1.100	-1.920

TABLE III. The calculated total magnetic moment m_{tot} , local magnetic moments residing on the Mo atoms $m_{Mo(1)}$, $m_{Mo(2)}$, $m_{Mo(3)}$ and $m_{Mo(4)}$ of the system with V_{Nin} under different strains.

Strain	m_{tot} (μ_B /super-cell)	$m_{Mo(1)}$ (μ_B /atom)	$m_{Mo(2)}$ (μ_B /atom)	$m_{Mo(3)}$ (μ_B /atom)	$m_{Mo(4)}$ (μ_B /atom)
-10%	0.000	0.000	0.000	0.000	0.000
-9%	0.946	0.380	0.380	0.380	-0.170
-8%	0.996	0.420	0.420	0.420	-0.190
-6%	1.000	0.460	0.460	0.460	-0.230
-4%	1.000	0.500	0.500	0.500	-0.280
-2%	1.000	0.540	0.540	0.540	-0.340
0	1.000	0.580	0.580	0.580	-0.410
2%	1.000	0.630	0.630	0.630	-0.520
4%	1.000	0.710	0.710	0.710	-0.690
6%	1.001	0.820	0.820	0.820	-0.970
8%	1.001	1.000	1.000	1.000	-1.430
10%	1.055	1.220	1.220	1.220	-1.930